Record-breaking Barents Sea Ice Loss Favors to the Unprecedented Summertime Extreme Heatwave in 2021 over Western North America by Enhancing Rossby Wave Ridge

Yuying Wei
Ocean University of China
Fei Huang
Ocean University of China
Zheng Chen (chenzhengouc@163.com)
Ocean University of China https://orcid.org/0000-0002-8727-8595

Research Article

Keywords: Extreme heatwave, Western North America, Rossby wave ridge, Barents sea ice loss, Circumglobal teleconnection, Jet steam

Posted Date: May 30th, 2023

DOI: https://doi.org/10.21203/rs.3.rs-2894029/v1

Abstract

A record-setting extreme heatwave occurred over western North America (WNA) in the summer of 2021, which was associated with an extreme atmospheric Rossby wave ridge (ARR) over WNA and a minimum record event of the pre-winter Barents Sea ice concentration. We identify the temporal-spatial remote effect and investigate how the sea ice loss in the Barents Sea modulates the intensity of the ARR and extreme heatwaves by analyzing the reanalysis data. Our results suggest that atmospheric wave activity flux associated with Barents Sea ice loss (BSIL) in pre-winter transferred wave energy towards the circumglobal teleconnection (CGT)-like wave trains, increasing the wave amplitude and enhancing the ARR over WNA. Meanwhile, the weakening of the jet streams drives atmospheric subsidence and increases the shortwave radiation, leading to anticyclonic anomalies over WNA and the enhancement of the ARR. Both the CGT-like wave trains and the weakened jet streams contribute to the synergistic effect of the enhancing ARR and more frequent extreme heatwaves. And the BSIL serves as a pioneer predictor for the predictions of extreme heatwaves 6 months in advance. The above analysis can improve the prediction skills of extreme heatwaves over WNA, possibly predicting more precisely.

1. Introduction

The summertime extreme heatwaves appear to be on the rise in the Northern Hemisphere as a result of climate change. The latest studies show that the mean spatial extent, maximum intensity duration, and frequency of the heatwaves have significantly increased under global warming (Perkins-Kirkpatrick and Lewis 2020; Rogers et al. 2022; McKinnon and Simpson 2022). The World Meteorological Organization reported that the temperatures reached a peak and broke the previous records in numerous cities across the United States and Canada in June 2021. With a temperature of 49.6°C (24°C higher than average), Lytton, British Columbia, Canada became the highest temperature ever recorded above 45 °N latitude worldwide according to Environment and Climate Change Canada. This extreme heatwave, which burned western North America (WNA) and Canada and caused huge economic losses and casualties, is around a once-in-a-millennium event (Ebi et al. 2021; Philip et al. 2021; Schramm et al. 2021; Henderson et al. 2022). Furthermore, along with the enhanced North Pacific sea surface temperature (SST) anomalies and atmospheric circulation variations under global warming, there will be more intense, more frequent and longer lasting heatwaves over WNA in the second half of the 21st century according to the future scenario runs of coupled climate models (Meehl and Tebaldi 2004; Chen et al. 2018; Chen et al. 2023). According to statistics, the extreme events show significant rising trends through time in both observational reanalysis datasets and projections of climate models (Bartusek et al. 2022; Thompson et al. 2022; Dong et al. 2023; Heeter et al. 2023; Lucarini et al. 2023).

Due to the enormous impact this extreme heatwave puts on human life, how to trigger such a devastating event and the occurrence mechanism have drawn more attention in recent years. In late June of 2021, a large tropospheric blocking ridge was established after the unstable polar vortex center split and allowed an omega block to form at the surface and persistent anticyclonic anomalies over northwestern states of the U.S. and Canada (Overland 2021; Zhou et al. 2022). This strong anomalous high-pressure system

over the WNA can explain half of the magnitude of the anomalous temperature (Zhang et al. 2023). Persistence of the blocking allowed increased radiation, low soil moisture and adiabatic subsidence, which jointly contributed to this heatwave over WNA (Neal et al. 2022; Schumacher et al. 2022; Thompson et al. 2022). The anomalous atmospheric river across the North Pacific and a Rossby wave train excited by weakened monsoon precipitation in East Asia both resulted in this extraordinary heatwave event (Lin et al. 2022; Mo et al. 2022; Qian et al. 2022; Terray 2023). Wang et al. (2023) demonstrate that greenhouse gases are the primary cause for the trend of daily maximum temperatures in WNA from the past to the future. The equatorward shifts and weakening of the zonal jet streams occur more frequently after global warming, which will lead to higher temperatures in WNA (Overland 2021; Philip et al. 2021). In the mid-latitudes, amplified quasi-stationary circumglobal Rossby waves associated with anomalous jet streams are more likely to cause extreme heatwaves in the Northern Hemisphere (Coumou et al. 2014; Lin and Yuan 2022). Human activities rise the maximum temperature of extreme heatwaves (King et al. 2016; Philip et al. 2021; Bercos-Hickey et al. 2022). And these extreme events tend to be more frequent in the summertime during La Niña years (Luo and Lau 2020). Meanwhile, the establishment of blocking contributes to enhancing radiative forcing, subsiding atmosphere and increasing diabatic heating, which all eventually lead to surface temperature rising (Zschenderlein et al. 2019). The formation and maintenance of the blockings are significantly influenced by synoptic-scale eddies, upstream latent heating and jet streams (Hoskins et al. 1983; Luo et al. 2001; Nakamura and Huang 2018; Kim and Lee 2022). However, the Eastern Pacific-North American region tends to experience blocking less frequently (Tibald et al. 1997). Therefore, there must be some other factors to explain the more frequent heatwaves in recent decades over North America.

The Arctic sea ice and snow cover have undergone unprecedented changes. Recent studies reveal that near-surface Arctic warming along with sea ice melting can modify the atmospheric circulation and weather-related factors, such as jet streams, meridional temperature gradient and storm tracks in the midlatitudes, which will contribute to amplifying the intensity and frequency of extreme weather and climate events (Francis and Vavrus 2012; Cohen et al. 2014; Barnes and Screen 2015). Meanwhile, the combined loss of sea ice and snow cover modulate interannual and subseasonal atmospheric variabilities in the midlatitudes and lead the extreme events (Honda et al. 2009; Deser et al. 2010; Tang et al. 2013; Vihma 2014; Gu et al. 2018; Chripko et al. 2021). The maintenance of the sea ice loss in the Arctic relies on local atmospheric and oceanic processes and self-supporting feedback spontaneously, such as sea ice thickness and concentration feedback, albedo feedback, snowfall feedback, cloud and water vapor feedback, and temperature feedback (Curry et al. 1995; Serreze et al. 2009; Screen and Simmonds 2010; Döscher et al. 2014; Zhou et al. 2022). Furthermore, sea ice variations make a significant contribution to the long-term prediction of weather and climate (Wu et al. 2009; Xing and Huang 2019; Zhu et al. 2019).

The atmospheric dynamics in midlatitudes are acknowledged as too chaotic to predict, but the atmospheric circulation variations, such as anomalous atmospheric planetary waves, are helpful to make heatwaves more predictable beyond the scope of the typical weather forecast (Teng et al. 2013). Extreme weather and climate predictions are of immense societal and economical benefit. Unfortunately, even

though most models were able to predict the above-normal temperature in the summer of 2021, the magnitude of the heatwave was severely underestimated (Emerton et al. 2022). Therefore, selecting the predictor related to specific atmospheric circulation variations has been a foremost challenge in predicting future changes in heatwave events. The extreme heatwave in the summer of 2021 over WNA has been reasonably addressed by weather-scale processes. Previous studies also focus on the analysis of the synoptic and subseasonal timescale predictors, which make extreme heatwaves unexpected in climate prediction.

Given all the evidence above, two questions need to be fully addressed in this paper. One is what causes such an extreme heatwave event that happened in the early summer of 2021. The other is whether there is any credible predictor to improve the accuracy of the heatwaves forecasts in case to reduce the hazard to human life. To answer these two questions, we have examined the historical extreme heatwaves and the related general circulation conditions over WNA. We also briefly discuss the sea ice loss in the previous winter favors the positive geopotential height (GPH) anomalies via the propagation of Rossby waves and the weakening zonal jet streams. The results show that the Barents Sea ice loss (BSIL) can forecast the extreme heatwaves 6 months in advance over WNA, which makes it a good predictor. The rest of the paper is organized as follows. Section 2 describes the datasets and analysis methods. In section 3, we illustrate the extreme heatwave event in the summer of 2021, and its relationship with the atmospheric Rossby wave ridge (ARR) in the WNA. The impact of BSIL along with the weakening jet streams on the ARR, both contribute to heatwaves over WNA are shown in section 4. A summary and discussion are given in section 5.

2. Datasets and methods

2.1. Data

One set of data used in this study is the National Center for Environmental Prediction/National Center for Atmospheric Research (NCEP/NCAR) reanalysis , with a horizontal of 2.5° × 2.5° (Kanamitsu et al. 2002). The daily and monthly atmospheric dataset includes surface air temperature at 2 meters, GPH and winds fields. The monthly sea ice concentration (SIC) dataset employed in our research is the Nimbus-7 SMMR and DMSP SSM/I-SSMIS Passive Microwave Data Version 2 distributed by NASA National Snow and Ice Data Center Distributed Active Archive Center (NSIDC DAAC) with the resolution of 25 kilometers, which is used to analyze the Rossby wave ridge over North America associated with the Arctic sea-ice loss (DiGirolamo et al. 2022).

Unless otherwise noted, the summertime discussed in this paper is from June to July (JJ) during 1979–2021. The anomalies are calculated by using this period of time as the climatology.

2.2. Index definitions

We define the index of the atmospheric Rossby wave ridge over WNA (I_{ARR}) to evaluate the variabilities of this high-pressure ridge. The normalized I_{ARR} is calculated by area (30°N -60 °N, 120°W -90 °W) averaging

of 500-hPa GPH anomalies (GPHa) in early summer. The area is selected by zonal deviation of 500-hPa GPH in climatology, which reflects the most active area of the ARR over WNA.

Likewise, the sea ice loss index (I_{SIL}) is calculated by averaging the opposite values of SIC anomalies in which region (78°N -83 °N, 12°E -78 °E) demonstrates the highest correlation coefficients with I_{ARR}. The I_{SIL} shows the opposite SIC variabilities, which is intuitionally interpreted as the variations of sea ice loss.

2.3. Analysis methods

The composite analysis is used in this study to demonstrate the spatial distribution of the anomalies of each variable to the normalized index. The composite patterns are obtained by averaging linear-detrended anomalies of those periods when the indices are below (above) one standard deviation as the positive (negative) phases. And we employ a student's t-test to assess the statistical significance of the differences between positive and negative composites.

The regression analysis is to demonstrate atmospheric variabilities associated with indices of the atmospheric activity. The regression patterns are extracted by regressing the detrended anomalies of the atmospheric fields (relative to the climatological mean for 1979–2021) onto the normalized indices.

The probability density functions (PDFs) of the air temperature maximums (T_{max}) are calculated to measure the intensities of extreme heatwave events (Stefanon et al. 2012). We have calculated the T_{max} of each day in early summer from 1979 to 2021 (43 years) as the cardinality. If there is a value that exceeds the upper 95th centile of the local PDF, we consider that there has been an extreme heatwave event that occurred that day. The magnitude above a threshold is the abnormal degree of the heatwave. And the abnormal degree turns into 0 if the value is not able to exceed the threshold. The sum of the abnormal degree of the heatwave in a month is used to comprehensively assess the frequency and magnitude of the heatwaves, which can be considered as the integrated intensity of the extreme heat events. We extract the abnormal degrees of June and July per year and turn that into a time series. Then we normalize the index and select the period when the index is above (below) one standard deviation to composite (none) extreme heatwave events.

2.4. Atmospheric wave activity flux

The atmospheric wave activity flux is employed in our research to illustrate the atmospheric wave activity associated with BSIL. To diagnose the propagation anomalies of atmospheric Rossby waves, the formula for calculating wave-activity flux derived by Takaya and Nakamura (2001) is as follows:

$$W = \frac{pcos\phi}{2\left|U\right|} \bullet \begin{pmatrix} \frac{U}{a^2cos^2\phi}\left[\left(\frac{\partial\Psi'}{\partial\lambda}\right)^2 - \Psi'\frac{\partial^2\Psi'}{\partial\lambda^2}\right] + \frac{V}{a^2cos\phi}\left[\frac{\partial\Psi'}{\partial\lambda}\frac{\partial\Psi'}{\partial\phi} - \Psi'\frac{\partial^2\Psi'}{\partial\lambda\partial\phi}\right] \\ \frac{U}{a^2cos\phi}\left[\frac{\partial\Psi'}{\partial\lambda}\frac{\partial\Psi'}{\partial\phi} - \Psi'\frac{\partial^2\Psi'}{\partial\lambda\partial\phi}\right] + \frac{V}{a^2}\left[\left(\frac{\partial\Psi'}{\partial\phi}\right)^2 - \Psi'\frac{\partial^2\Psi'}{\partial\phi^2}\right] \end{pmatrix}, (1)$$

where p is the normalized atmospheric pressure (pressure per 1000 hPa), U (= $(U,V)^{\mathrm{T}}$) indicate the average climatic wind fields, |U| is the speed of the climatological mean winds, Ψ' is the perturbation stream function, a is the earth's radius, N^2 is the buoyancy frequency squared, and φ and λ denote latitude and longitude, respectively.

Here the perturbation geostrophic stream function (Ψ') is also employed to illustrate the influence of SIL on the Rossby wave trains. The seasonally averaged 500-hPa geostrophic stream function anomalies are calculated relative to the climatological mean from 1979 to 2021. The formula for calculating geostrophic stream function (Ψ) is as follows:

$$\Psi = \frac{\Phi}{f}, (2)$$

Where Φ is 500-hPa geopotential height and f (= $2\Omega\sin\varphi$) is the Coriolis parameter. Then we use the stream function anomalies regressing onto the I_{SIL} to reveal the perturbation stream function induced by SIL.

3. Connection between heatwaves and the ARR over WNA

3.1 The unprecedented extreme heatwave event over WNA in the summer of 2021

In the early summer of 2021, a record-setting heatwave occurred in WNA. As reanalysis data shown in Fig. 1a, the six hours mean temperatures are all over 37°C from June 14th to 18th, 2021 with a maximum of 39.8°C (17.1°C higher than climatology) in California, America (the triangle mark in Fig. 1b). The World Meteorological Organization has defined a weather process in which the daily maximum temperature exceeds 32°C for over 3 days as a heatwave event. There were 6 times heatwaves (42 days above 32°C) in early summer (JJ), and the average climatology is below 25°C during this time, which made the heatwaves more intense than the late summer. Such extreme heatwaves in the early summer of 2021 affected numerous unprepared people and caused hundreds of deaths (Philip et al. 2021). Therefore, we primarily discuss the heatwaves and the related factors during early summer (JJ) through this article.

The horizontal structure of the GPHa and surface winds anomalies during the early summer of 2021 are shown in Fig. 1b. Note that the robust high-pressure anomalies collaborated with strong anticyclone anomalies have been taken over WNA at that time, which strengthens the intensity of the high-pressure ridge. The maximum GPHa reaches 73.3 gpm. Such conditions trigger the summer blocking high, which usually contributes to the persistence of heatwave events. There are southeasterly anomalies near California compared to the climatological westerly to southwesterly, which leads to less cold and wet advection transport to this area.

The anomalies along with the climatology of the temperature and GPH over North America in the summer of 2021 are demonstrated in Fig. 2a and 2b Hovmöller diagrams respectively. There are usually two warm centers located at 95 °W and 115 °W in July, and the temperature of the eastern center is higher than the western one. But in the early summer of 2021, the warm anomalies mainly distribute in the west, with a large area of cool anomalies over the southern U.S. The dipole structure is the principal mode of heatwave variability over North America (Yu et al. 2023). And the eastern one shows below-normal anomalies in late June and early July. Such a phenomenon is highly correlated with the variations of GPH. As shown in Fig. 2b, the quasi-stationary Rossby wave ridge centered at 100 °W moving westward (110 °W) during 12–16 June, and one week later on 21–30 June, a blocking high is maintained and centered at 120°W. The conditions of GPHa are in favor of warm extremes and causing the heatwaves during 14–20 June and 26 June to 14 July, which centers moving from 100 °W to 115 °W and quasi-stationary centered at 120 °W. These heatwaves are one month in advance of the hottest period in the WNA, which brings a great disaster to unprepared people.

Historically, the summertime warm center in Fig. 2c is usually at 100 °W and the synchronous high-pressure ridge in Fig. 2d is around 110 °W. When the ridge goes higher, for instance, in 1987, 2005, 2016, etc., it shifts westward, which causes the warm center hotter and further west. In the summer of 2021, the GPH is much higher than the historical records and significantly shifting westward from climatology, which leads to the record-setting extreme heatwave that occurred in WNA. As Hovmöller shows, the positive GPH anomalies are highly related to the heatwave events in summer. The temperature response to high-pressure anomalies is consistent with previous studies on heatwaves that occurred in Europe (Black et al. 2004; Zschenderlein et al. 2019). Therefore, we need to measure the variations of the summertime ridge which is highly related to the heatwaves over WNA next.

3.2 Frequent extreme heatwaves induced by ARR over WNA

The horizontal structures of the climatological winds and GPH in early summer for 1979–2021 are shown in Fig. 3a. To portray the variations of the ARR over WNA, we calculate the zonal deviations of the latitudes and select the appropriate area (30°N -60 °N, 120°W -90 °W) to compute the ARR index I_{ARR} (see Section 2.2 for details). The normalized I_{ARR} and synchronous air temperature (TA) index calculated by averaging the temperature anomalies in the same region with the ARR index are displayed in Fig. 3b. There are robust and similar uptrends along with interannual variabilities in both indices. Note that global warming and anthropogenic forcing result in warming and thermal expansion of the lower atmosphere, which leads to linear uptrends (Christidis and Stott 2015). The I_{ARR} in 2021 reached its maximum since 1979. The ARR features a maximum of ~ 5980 gpm in June 2021, which is unprecedented for the WNA since 1979 (Overland 2021). The TA index in 2021 also rises to the highest in 43 years of reanalysis data. The correlation coefficient between I_{ARR} and the TA index is 0.89 on the 0.01 significance level, which confirms the relative role of ARR to the heatwave events in early summer over WNA.

In case to further confirm the level of the heatwave influenced by the intensity of ARR, we employ composite analysis and PDFs to reveal the correspondence between temperature and pressure variations

(see Section 2.3 for details). As displayed in Fig. 4a, the integrated temperature anomalies which exceed the upper 95th centile of the local PDFs are located in the Midwest of North America when ARR demonstrates above-normal anomalies. And the maximum values are just in the area where we select to measure the variations of ARR. On the contrary, there is no heatwave event relevant to the weakening of ARR in central and WNA (Fig. 4b). Only the Alaska region has a slight connection with it. Therefore, we have confirmed that the extreme heatwaves are consistent with the enhancement of the ARR over WNA. The anticyclonic winds anomalies and atmospheric subsidence make the temperature rise through adiabatic heating and shortwave radiation. The heat budget results for the heatwaves confirm the contribution of the adiabatic heating process within the anticyclone dominating the heatwaves over North America (Qian et al. 2022). As we find that extreme heatwaves are more likely to take place in WNA when the ARR is enhanced. Next, we need to focus on the mechanism of the ARR variations and find the factors or even better predictors to cause I_{ARR} changes.

4 Record-breaking Barents Sea Ice Loss Favors to the enhanced Rossby wave ridge over WNA

4.1 Barents Sea ice loss in previous winter relevant to the ARR over WNA in early summer

In the early winter of 2021, the Barents-Laptev sea ice reached a minimum for the period 1981–2020 and reduced the meridional gradient (Yang and Fan 2022). In this section, we further reveal the potential roles of the Arctic sea ice anomalies in the changes of ARR intensities over WNA. The correlation patterns between I_{ARR} and SIC of the Arctic Ocean in previous winter, spring and synchronous summer are shown in Fig. 5. The patterns demonstrate the significant negative correlation between I_{ARR} and SIC from previous winter to summer in the Barents Sea area where displays the minimum correlation coefficients down to -0.60 Wang et al. (2022) indicate that the sea ice loss in the summertime Chukchi Sea is a factor which causes more frequent quasi-barotropic ridges and more devastating heatwaves over WNA. However, the SIC anomalies in the Barents Sea in the pre-winter related to summertime ARR over WNA and lasted for more than half a year, which might be a good predictor for the heatwaves and explain such an extreme heatwave event in 2021. The SIC in the Chukchi Sea seems correlated with ARR in winter, but the correlation coefficients are not as significant as that in the Barents Sea. Also the signless SIC in Chukchi Sea in spring means the SIC in summer may not contain the signal from the previous winter, which cannot make SIC in Chukchi Sea a predictor.

The wintertime sea ice melting in the Barents Sea can last till early summer by different positive feedbacks. The positive ice-albedo feedback will amplify the initial warming and sea ice retreat (Curry et al. 1995). For instance, the Barents Sea ice feedback usually reaches its peak in winter and spring (Koenigk et al. 2009). Less sea ice in winter will postpone the freezing processes and make the thinner of ice (Zhou et al. 2022). The thinner sea ice would shrink faster to intensify the ice-albedo feedback (Parkinson and Washington 1979). The reduced SIC and thickness at the end of winter could lead to more melting in summer. So the SIC anomalies in winter will last for more than six months after accelerated

melting in spring, which explains what makes sea ice loss in pre-winter the leading signal of the ARR in summer.

Due to the thermal inertia of the sea ice, we find that the I_{ARR} is highly related to the variabilities of SIC in the Barents Sea from previous winter to summer. The signal preserves in the sea ice for long memory, which makes it a good predictor. Thus, we select the Barents Sea region (78°N -83 °N, 12°E -78 °E; green box in Fig. 5) and calculate I_{SIL} (See Section 2.2 for details). Note that the I_{SIL} is the negative area-averaging value of SIC, which is used to measure the melting of sea ice in the Barents Sea. Normalized I_{SIL} in pre-winter, spring and early summer are shown in Fig. 6 with the rising trends. The correlation coefficient between I_{SIL} in early summer and pre-winter is 0.75 on the 0.01 significance level. As the similar variations of I_{SIL} in three seasons, we choose the I_{SIL} in pre-winter as the predictor to study its relative roles with ARR over WNA. Unless otherwise noted, the I_{SIL} refers to the variations of BSIL in pre-winter (DJF). According to the extreme heatwave in 2021, we find I_{SIL} in the pre-winter reaching its maximum. The correlation between I_{ARR} and the pre-wintertime I_{SIL} is 0.62 ($p < 0.01$). The results indicate that the SIC will serve as a predictor of ARR which eventually leads to extreme heatwave events. Previous studies focused on the synchronous factors causing heatwaves but ignored the possibility of predictors. By using I_{SIL}, we could make the heatwaves taking place in WNA more predictable at least six months in advance. In this case, we should look into the mechanism of the relative role between BSIL and ARR more deeply.

4.2 Way of BSIL on the enhanced ARR via circumglobal teleconnection

To better understand the relative role of BSIL on the ARR, we regress the summertime 500-hPa GPHa onto the I_{SIL} (Fig. 7a). The regression pattern shows the spatial feature of the circumglobal teleconnection (CGT) -like pattern in the midlatitudes. The CGT pattern identifies the leading mode of summertime GPHa in the northern hemisphere (Ding and Wang 2005). The results indicate that BSIL triggers CGT-like wave trains that contribute to the enhancing ARR and lead to increasing extreme heatwaves over WNA. The regressed 500-hPa GPHa onto the summertime I_{ARR} shows a similar pattern to Fig. 7a (not shown). Therefore, the BSIL will sustainedly affect the summertime general circulation since pre-winter.

To further understand the role of SIL on the ARR and heatwaves, we construct the composite patterns by $I_{SIL} > 0.8$ (Fig. 7b) and $I_{SIL} < -0.8$ (Fig. 7c). We find the asymmetry patterns when comparing these two composites. During the period of BSIL, the robust CGT-like pattern (similar pattern as in Fig. 7a) is triggered and the positive anomalies center in WNA that is related to ARR is significantly enhanced, which explains the consistent extreme heatwaves with the ARR (Fig. 4a). However, the ARR center is not shown decrease robustly when sea ice of the Barents increases. This is because the increasing sea ice still has a profound influence on the atmospheric circulation by a westerly jet waveguide forming an opposite phase shift CGT-like pattern in which center locations and intensities are different. Note that generally the ARR is

weakened and the center near Alaska is enhanced, which explains the heatwave events only occurred in Alaska region but not in WNA (Fig. 4b).

Next, we use 500-hPa atmospheric T-N wave activity flux (see Section 2.4 for details) to demonstrate the contributions of the sea ice in the Barents Sea to the general circulation. We draw the atmospheric wave activity patterns in June (Fig. 8a) and July (Fig. 8b), which are relative to BSIL. The pattern in June is clearly shown that there are Rossby wave disturbances in the Barents Sea that transmit to the Siberian, the source center of the CGT-like pattern, which increases the amplitude of each center through the Rossby wave trains and eventually enhances the ARR. Besides, as shown in Fig. 8b, the CGT-like wave trains shift northeastward in July, which explains why the eastern center of temperature maximum is higher than the western one in July (Fig. 2a and 2c). The anomalous energy of the Arctic melting sea ice disperses downstream and modulates the atmospheric circulation through wave-current interactions, which resulted in the enhancement of ARR. In June 2021, there were two unexpected extreme heatwaves occurred. And we compute the T-N wave activity flux patterns of these two events during 12-16th (Fig. 8c) and 21-30th (Fig. 8d) June 2021, respectively. The perturbation wave source in the Barents Sea emanates wave activity flux southeastward to the positive source center of a CGT-like pattern and then enhances the ARR during the first process in 2021. The second heatwave process shows that the amplification of the ARR amplitude in the late June of 2021 was mainly due to a relay Rossby wave source originating from the North Pacific, one of the negative centers of the CGT wave trains.

4.3 Role of the weakened jet streams induced by BSIL on the enhancement of ARR

Weakened high-level jet streams usually increase the amplitude of ARR through the energy cascade of wave-flow interaction. A recent study finds that the weakening of the zonal winds in the Eurasian continent is significantly influenced by the Arctic amplification effect through Arctic-midlatitude temperature contrasts modulation (Wang et al. 2017). The melting of the sea ice in the Arctic will reduce the meridional temperature gradient. The polar-equatorial temperature gradient in the Northern Hemisphere has significantly decreased in the past, which may explain the linear uptrend of ARR. In our study, the 200-hPa zonal winds associated with BSIL turn weaker and the westerly jet core breaks over the WNA in June (Fig. 9a) and July (Fig. 9b). It indicates that the negative zonal winds anomalies are in favor of the development and persistence of the high-pressure system. The jet stream belt in 30–40 °N is significantly weakened in July, which leads to the stagnation of the weather systems and eventually enhances the ARR (Fig. 9b). The weakened jet stream in this region indicates that the transmission of energy is from the mean flow to the synoptic scale perturbations through wave-mean flow interaction. The synoptic-scale energy accumulates in the convergence of the wave activity flux over North America, which donates the enhancement of the ARR (Fig. 8).

In addition, we draw the zonal wind patterns during two extreme heatwave processes (Fig. 9c and 9d). The first heatwave process shows the weakened jet stream in the WNA. Combined with the enhanced center of CGT-like pattern associated with the BSIL makes the intensity of ARR amplified in 2021 (Fig. 8c).

During the second event, the zonal winds are significantly weakened over the western coast of North America, which is consistent with the convergences of wave flux in WNA in the late June of 2021 (Fig. 8d), suggesting the enhancement of the ARR and leading to the extreme heatwave.

It is noted that a north-south dipole anomaly zonal wind pattern with a westerly anomaly in the north and easterly anomaly in the south always appears in the gap region of the jet stream core over the WNA (Fig. 9a, c, d). This dipole zonal wind anomaly pattern favors a high-level anticyclone geopotential height anomaly consistent with sinking airflow and ARR over the WNA (Fig. 7a). In a word, weakened high-level westerly jet induced by BSIL plays an important role in enhancing ARR by atmospheric jet stream dynamics.

5. Summary and discussion

The research elucidates the relative roles of BSIL in the variations of the Rossby wave ridge over WNA in early summer, which eventually causes heatwave events. According to observational reanalysis, a record-setting extreme heatwave occurred over WNA in the summer of 2021. Meanwhile, we noticed that the intensity of the ARR in WNA also reached the extreme. The composite analysis showed that extreme heatwaves are more likely to take place in WNA when the ARR is enhanced. The ARR leads to extreme heatwaves by increasing atmospheric subsidence and shortwave radiation. We also found that the Barents Sea ice also set a minimum record in SIC just in the pre-winter ahead of the 2021 summertime heatwaves. For the thermal inertia of the sea ice, we have demonstrated the BSIL index I_{ARR} closely associated with variabilities of Barents Sea ice from the previous winter to synchronous summer, which makes the Barents Sea ice a performance predictor 6 months in advance. The impacts of BSIL on the ARR and summertime extreme heatwaves are driven by two pathways: (a) atmospheric wave activity flux associated with BSIL in pre-winter will transfer wave energy towards the CGT-like wave trains, which increases the amplitude of pattern and enhances the ARR over WNA; (b) the weakening of the jet streams drive atmospheric subsidence and increases the shortwave radiation, which leads to the anticyclonic anomalies over WNA and the enhancement of the ARR. Both the CGT-like wave trains and the weakened jet streams contribute to the enhancing ARR and more frequent extreme heatwaves.

Our study identifies a temporal-spatial remote effect between the variations of Barents Sea ice in pre-winter and the Rossby wave ridge over WNA in summer. The synergistic effect of the BSIL induced CGT-like wave trains and the weakened jet streams that cause the enhancing ARR and extreme heatwaves are summarized schematically as in Fig. 10. According to the physical mechanism, the extreme heatwaves over WNA will possibly predict more precisely in advance.

Heatwave events vary in their forcing mechanisms and connections to large-scale climate modes. We also have explored the influence of other factors such as the variabilities of the North Pacific SST on the heatwave events over North America, but there are no robust results or significant signals that have been revealed. The researches on the coupled ice-atmospheric processes are necessary to carry a deep understanding of the diverse roles of extreme heatwaves under a warming climate.

Declarations

Acknowledgments

Authors are thankful to the anonymous reviewers whose comments and suggestions have helped us to improve the overall quality of the manuscript. We acknowledge the NCEP and NSIDC for producing and making available their datasets.

Funding

This work was supported by the National Key Research and Development Program of China (2019YFA0607004), National Natural Science Foundation of China (NSFC) Projects (42006017, 42075024, 42075025), and Natural Science Foundation of Shandong Province (ZR2019ZD12), Taishan Pandeng Scholar Project.

Availability of data and material

The daily and monthly mean NCEP-NCAR reanalysis data can be downloaded from https://psl.noaa.gov/data/gridded/data.ncep.reanalysis2.html. The monthly mean SIC data can be obtained at https://nsidc.org/data/nsidc-0051/versions/2.

Conflict of interest

The authors have not disclosed any competing interests.

References

1. Barnes EA, Screen JA (2015) The impact of Arctic warming on the midlatitude jet-stream: can it? Has it? Will it? Wiley Interdiscip Rev Clim Change 6:277–286
2. Bartusek S, Kornhuber K, Ting M (2022) 2021 North American heatwave amplified by climate change-driven nonlinear interactions. Nat Clim Chang 12:1143–1150
3. Bercos-Hickey E, O'Brien TA, Wehner MF, Zhang L, Patricola CM, Huang H, Risser MD (2022) Anthropogenic contributions to the 2021 Pacific northwest heatwave. Geophys Res Lett 49(23):e2022GL099396
4. Black E, Blackburn M, Harrison G, Hoskins B, Methven J (2004) Factors contributing to the summer 2003 European heatwave. Weather 59(8):217–223
5. Chen Z, Gan B, Huang F et al (2023) The influence of Pacific-North American teleconnection on the North Pacific SST anomalies in wintertime under the global warming. Clim Dyn 60:1481–1494
6. Chen Z, Gan B, Wu L, Jia F (2018) Pacific-North American teleconnection and North Pacific Oscillation: historical simulation and future projection in CMIP5 models. Clim Dyn 50:4379–4403
7. Chripko S, Msadek R, Sanchez-Gomezet E et al (2021) Impact of reduced Arctic sea ice on Northern Hemisphere climate and weather in autumn and winter. J Clim 34:5847–5867

8. Christidis N, Stott PA (2015) Changes in the geopotential height at 500 hPa under the influence of external climatic forcings. Geophys Res Lett 42:10798–10806
9. Cohen J, Screen J, Furtado J et al (2014) Recent Arctic amplification and extreme mid-latitude weather. Nat Geosci 7:627–637
10. Coumou D, Petoukhov V, Rahmstorf S, Petri S, Schellnhuber HJ (2014) Quasi-resonant circulation regimes and hemispheric synchronization of extreme weather in boreal summer. Proc Natl Acad Sci 111(34):12331–12336
11. Curry JA, Schramm JL, Ebert EE (1995) Sea ice-albedo climate feedback mechanism. J Clim 8:240–247
12. Deser C, Tomas R, Alexander M, Lawrence D (2010) The seasonal atmospheric response to projected Arctic sea ice loss in the late twenty-first century. J Clim 23:333–351
13. DiGirolamo N, Parkinson CL, Cavalieri DJ, Gloersen P, Zwally HJ (2022) Sea ice concentrations from Nimbus-7 SMMR and DMSP SSM/I-SSMIS passive microwave data, version 2 [Data Set]. Boulder, Colorado USA.NASA National Snow and Ice Data Center Distributed Active Archive Center
14. Ding Q, Wang B (2005) Circumglobal teleconnection in the Northern Hemisphere summer. J Clim 18(17):3483–3505
15. Dong Z, Wang L, Xu P, Cao J, Yang R (2023) Heatwaves similar to the unprecedented one in summer 2021 over western North America are projected to become more frequent in a warmer world. Earths Future 11(2):e2022EF003437
16. Döscher R, Vihma T, Maksimovich E (2014) Recent advances in understanding the arctic climate system state and change from a sea ice perspective: a review. Atmos Chem Phys 14:13571–13600
17. Ebi KL, Capon A, Berry P et al (2021) Hot weather and heat extremes: health risks. Lancet 398(10301):698–708
18. Emerton R, Brimicombe C, Magnusson L et al (2022) Predicting the unprecedented: forecasting the June 2021 Pacific northwest heatwave. Weather 77(8):272–279
19. Francis JA, Vavrus SJ (2012) Evidence linking Arctic amplification to extreme weather in mid-latitudes. Geophys Res Lett 39(6):L06801
20. Gu S, Zhang Y, Wu Q, Yang XQ (2018) The linkage between Arctic sea ice and midlatitude weather: In the perspective of energy. J Geophys Res Atmos 123(20):11536–11550
21. Heeter KJ, Harley GL, Abatzoglou JT et al (2023) Unprecedented 21st century heat across the Pacific Northwest of North America. Clim Atmos Sci 6:5
22. Henderson SB, McLean KE, Lee MJ, Kosatsky T (2022) Analysis of community deaths during the catastrophic 2021 heat dome. Environ Epidemiol 6(1):e189
23. Honda M, Inoue J, Yamane S (2009) Influence of low Arctic sea-ice minima on anomalously cold Eurasian winters. Geophys Res Lett 36:L08707
24. Hoskins BJ, James IN, White GH (1983) The shape, propagation and mean-flow interaction of large-scale weather systems. J Atmos Sci 40(7):1595–1612

25. Kanamitsu M, Ebisuzaki W, Woollen J, Yang S-K, Hnilo JJ, Fiorino M, Potter GL (2002) NCEP-DOE AMIP-II reanalysis(R-2). Bull Am Meteorol Soc 83:1631–1643
26. Kim DW, Lee S (2022) Dynamical mechanism of the summer circulation trend pattern and surface high temperature anomalies over the Russian far east. J Clim 35(19):6381–6393
27. King AD, Black MT, Min S-K, Fischer EM, Mitchell DM, Harrington LJ, Perkins-Kirkpatrick SE (2016) Emergence of heat extremes attributable to anthropogenic infuences. Geophys Res Lett 43(7):3438–3443
28. Koenigk T, Mikolajewicz U, Jungclaus JH, Kroll A (2009) Sea ice in the Barents Sea: seasonal to interannual variability and climate feedbacks in a global coupled model. Clim Dyn 32:1119–1138
29. Lin H, Mo R, Vitart F (2022) The 2021 Western North American heatwave and its subseasonal predictions. Geophys Res Lett 49(6):e2021GL097036
30. Lin Q, Yuan J (2022) Linkages between amplified quasi-stationary waves and humid heat extremes in Northern Hemisphere midlatitudes. J Clim 35(24):8245–8258
31. Lucarini V, Galfi VM, Messori G, Riboldi J (2023) Typicality of the 2021 western North America summer heatwave. Environ Res Lett 18:015004
32. Luo D, Huang F, Diao Y (2001) Interaction between antecedent planetary-scale envelope soliton blocking anticyclone and synoptic-scale eddies: observations and theory. J Geophys Res Atmos 106(D23):31795–31815
33. Luo M, Lau N (2020) Summer heat extremes in northern continents linked to developing ENSO events. Environ Res Lett 15:074042
34. McKinnon KA, Simpson IR (2022) How unexpected was the 2021 Pacific Northwest heatwave? Geophys Res Lett 49(18):e2022GL100380
35. Meehl GA, Tebaldi C (2004) More intense, more frequent, and longer lasting heat waves in the 21st Century. Science 305(5686):994–997
36. Mo R, Lin H, Vitart F (2022) An anomalous warm-season trans-Pacific atmospheric river linked to the 2021 western North America heatwave. Comm Earth Environ 3:127
37. Nakamura N, Huang CSY (2018) Atmospheric blocking as a traffic jam in the jet stream. Science 361(6397):42–47
38. Neal E, Huang CSY, Nakamura N (2022) The 2021 Pacific Northwest heat wave and associated blocking: meteorology and the role of an upstream cyclone as a diabatic source of wave activity. Geophys Res Lett 49(8):e2021GL097699
39. Overland JE (2021) Causes of the record-breaking Pacific Northwest heatwave, late June 2021. Atmosphere 12(11):1434
40. Parkinson CL, Washington WM (1979) A large-scale numerical model of sea ice. J Geophys Res 84:311–337
41. Perkins-Kirkpatrick SE, Lewis SC (2020) Increasing trends in regional heatwaves. Nat Commun 11:3357

42. Philip SY, Kew SF, van Oldenborgh GJ et al (2021) Rapid attribution analysis of the extraordinary heatwave on the Pacific coast of the US and Canada June 2021.Earth Syst Dyn1–34
43. Qian Y, Hsu C, Yuan J, Zhu Z, Wang H, Duan M (2022) Effects of subseasonal variation in the east Asian monsoon system on the summertime heat wave in western North America in 2021. Geophys Res Lett 49(8):e2021GL097659
44. Rogers CDW, Kornhuber K, PerkinsKirkpatrick SE, Loikith PC, Singh D (2022) Sixfold increase in historical northern hemisphere concurrent large heatwaves driven by warming and changing atmospheric circulations. J Clim 35(3):1063–1078
45. Schramm PJ, Vaidyanathan A, Radhakrishnan L, Gates A, Hartnett K, Breysse P (2021) Heat-related emergency department visits during the northwestern heat wave - United States, June 2021. MMWR Morb Mortal Wkly Rep 70(29):1020–1021
46. Schumacher DL, Hauser M, Seneviratne SI (2022) Drivers and mechanisms of the 2021 Pacific Northwest heatwave. Earths Future 10(12):e2022EF002967
47. Screen JA, Simmonds I (2010) The central role of diminishing sea ice in recent Arctic temperature amplifification. Nature 464(7293):1334–1337
48. Serreze MC, Barrett AP, Stroeve JC, Kindig DN, Holland MM (2009) The emergence of surface-based Arctic amplifification. Cryosphere 3:11–19
49. Stefanon M, D'Andrea F, Drobinski P (2012) Heatwave classification over Europe and the Mediterranean region. Environ Res Lett 7:014023
50. Tang Q, Zhang X, Yang X, Francis JA (2013) Cold winter extremes in northern continents linked to Arctic sea ice loss. Environ Res Lett 8:014036
51. Takaya K, Nakamura H (2001) A formulation of a phase-independent wave-activity flux for stationary and migratory quasigeostrophic eddies on a zonally varying basic flow. J Atmos Sci 58(6):608–627
52. Teng H, Branstator G, Wang H, Meehl GA, Washington WM (2013) Probability of US heat waves affected by a subseasonal planetary wave pattern. Nat Geosci 6:1056–1061
53. Tibaldi S, D'Andrea F, Tosi E, Roeckner E (1997) Climatology of Northern Hemisphere blocking in the ECHAM model. Clim Dyn 13(9):649–666
54. Terray L (2023) A storyline approach to the June 2021 northwestern North American heatwave. Geophys Res Lett 50(5):e2022GL101640
55. Thompson V, Kennedy-Asser AT, Vosper E et al (2022) The 2021 western North America heat wave among the most extreme events ever recorded globally. Sci Adv 8(18):eabm6860
56. Vihma T (2014) Effects of Arctic sea ice decline on weather and climate: A Review. Surv Geophys 35:1175–1214
57. Wang C, Zheng J, Lin W, Wang Y (2023) Unprecedented heatwave in western North America during late June of 2021: roles of atmospheric circulation and global warming. Adv Atmos Sci 40:14–28
58. Wang H, Gao Y, Wang Y, Sheng L (2022) Arctic sea ice modulation of summertime heatwaves over western North America in recent decades. Environ Res Lett 17:074015

59. Wang Y, Huang F, Fan T (2017) Spatio-temporal variations of Arctic amplification and their linkage with the Arctic oscillation. Acta Oceanol Sin 36:42–51
60. Wu B, Zhang R, Wang B, D'Arrigo R (2009) On the association between spring Arctic sea ice concentration and Chinese summer rainfall. Geophys Res Lett 36:L09501
61. Xing W, Huang F (2019) Improvements in long-lead prediction of early-summer subtropical frontal rainfall based on Arctic sea ice. J Ocean Univ China 18(3):542–552
62. Yang H, Fan K (2022) Reversal of monthly East Asian winter air temperature in 2020/21 and its predictability. Atmos Ocean Sci Lett 15(1):100142
63. Yu B, Lin H, Mo R et al (2023) A physical analysis of summertime North American heatwaves. Clim Dyn. https://doi.org/10.1007/s00382-022-06642-1
64. Zhang X, Zhou T, Zhang W et al (2023) Increased impact of heat domes on 2021-like heat extremes in North America under global warming. Nat Commun 14:1690
65. Zhou T, Zhang W, Zhang L et al (2022) 2021: A year of unprecedented climate extremes in Eastern Asia, North America, and Europe. Adv Atmos Sci 39:1598–1607
66. Zhou X, Wang B, Huang F (2022) Evaluating sea ice thickness simulation is critical for projecting a summer ice-free Arctic Ocean.Environ Res Lett17(11)
67. Zhu Z, Huang F, Xie X (2019) Predictability of Chinese summer extreme rainfall based on Arctic sea ice and tropical sea surface temperature. J Ocean Univ China 18(3):626–632
68. Zschenderlein P, Fink AH, Pfahl S, Wernli H (2019) Processes determining heat waves across different European climates. Q J R Meteorol Soc 145:2973–2989

Figures

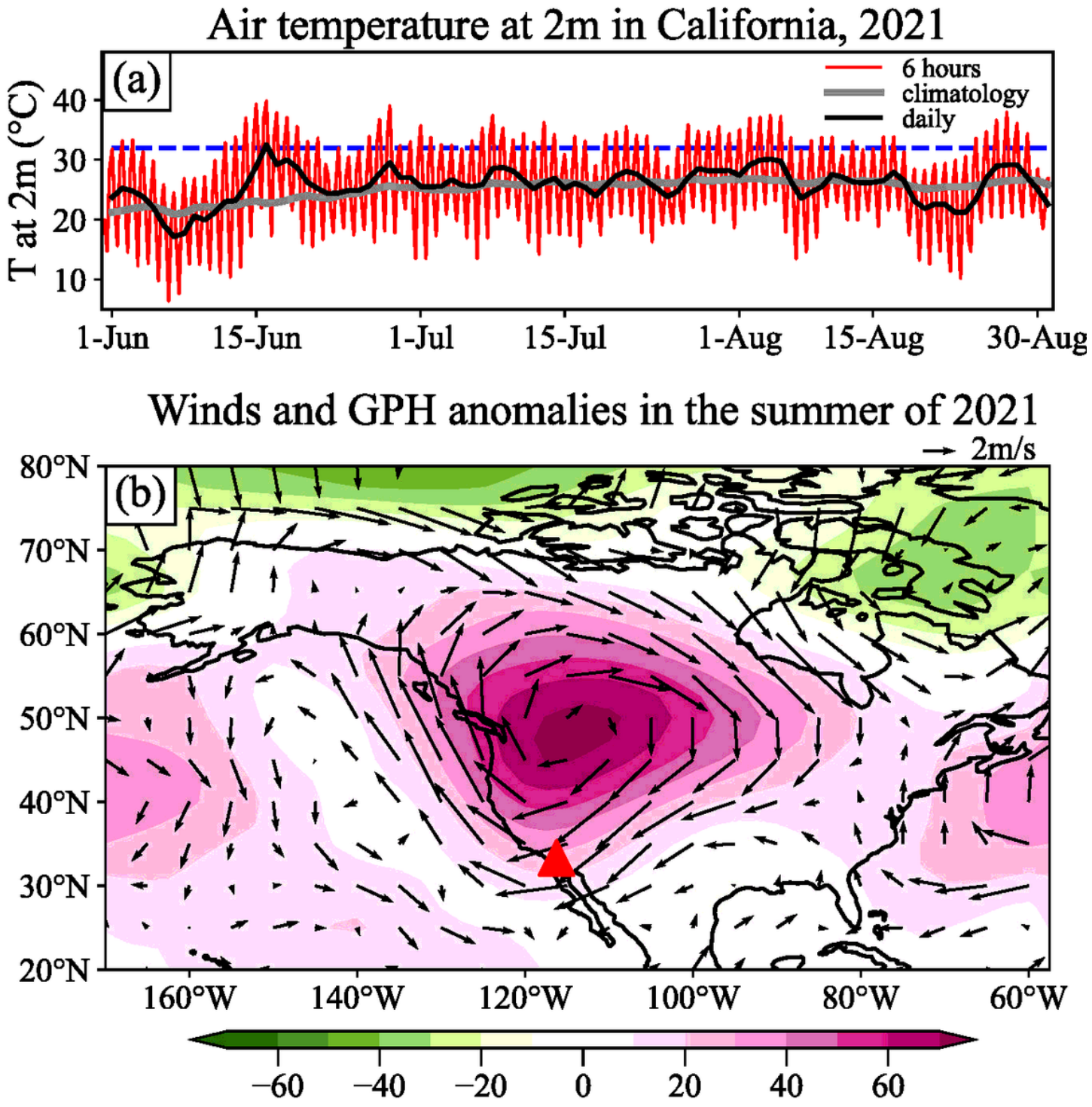

Figure 1

Illustration of the extreme heatwave over western North America in the summer of 2021. (a) The air temperature at 2 m in California (the location marked with a red triangle in Fig.1b) in the summer of 2021. The every 6 hours (red line), daily running mean (black line), and climatology (1979-2021; gray line) of the temperature are shown in this graph, respectively. Note that the reference line (blue dotted line) at 32 °C is regularly used to measure the heatwave events. (b) The GPH and winds anomalies over North America in

the summer of 2021. The 500-hPa winds and GPH anomalies are shown in vectors (units: m/s) and shading (units: gpm; interval: 10 gpm) respectively.

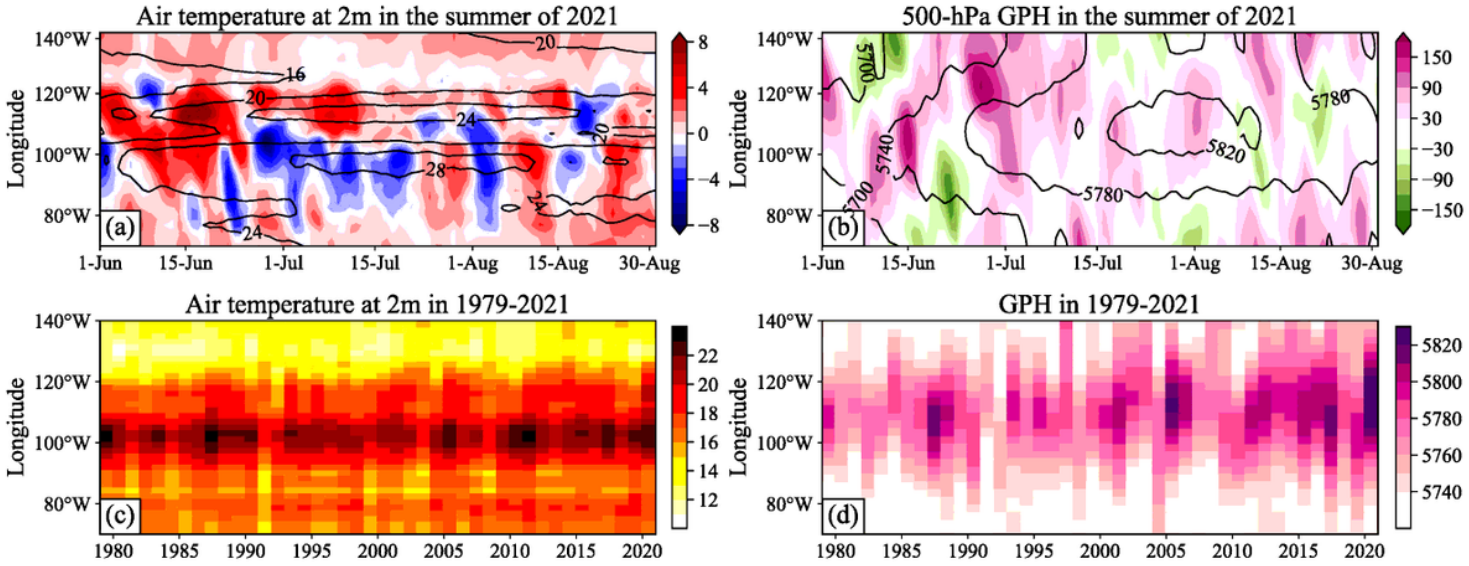

Figure 2

Hovmöller (time-latitude) diagrams of air temperature at 2 m (30°N -40 °N mean) and 500-hPa GPH (30°N -60 °N mean). (a) The temperature anomalies and climatology in the summer of 2021 are shown in shading (units: °C; interval: 1 °C) and contour (interval: 4 °C), respectively. (b) As in (a), but for GPH anomalies (shading, units: gpm; interval: 30 gpm) and climatology (contour, interval: 40 gpm). (c) The temperature (shading, interval: 1 °C) in summer for 1979-2021. (d) As in (c), but for GPH (shading, interval: 10 gpm).

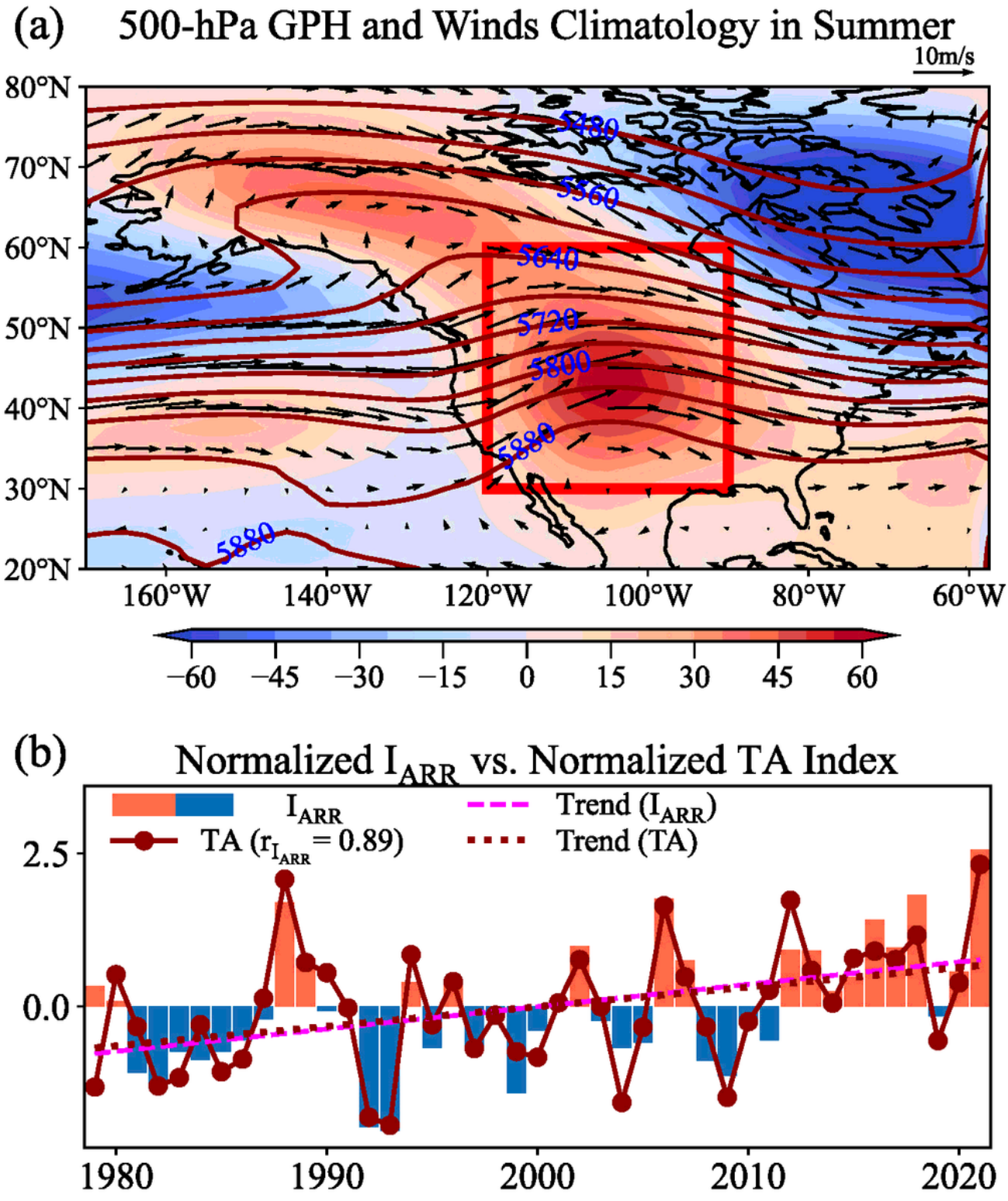

Figure 3

(a) The zonal deviations of 500-hPa GPH (shading; units: gpm; interval: 5 gpm) along with the mean climatological winds (vectors; units: m/s) and GPH (contour; interval 40 gpm) in the summertime. The region (30°N -60 °N, 120°W -90 °W) selected for calculating I_{ARR} and TA index in Fig. 3b is marked with a red box. (b) The normalized I_{ARR} is marked with red (positive) and blue (negative) bars along with its

linear trend (magenta dashed line), the same with the normalized TA index (kermesinus line) and the linear trend (kermesinus dotted lines). The correlation (r) between these two indices is 0.89 ($p<0.01$).

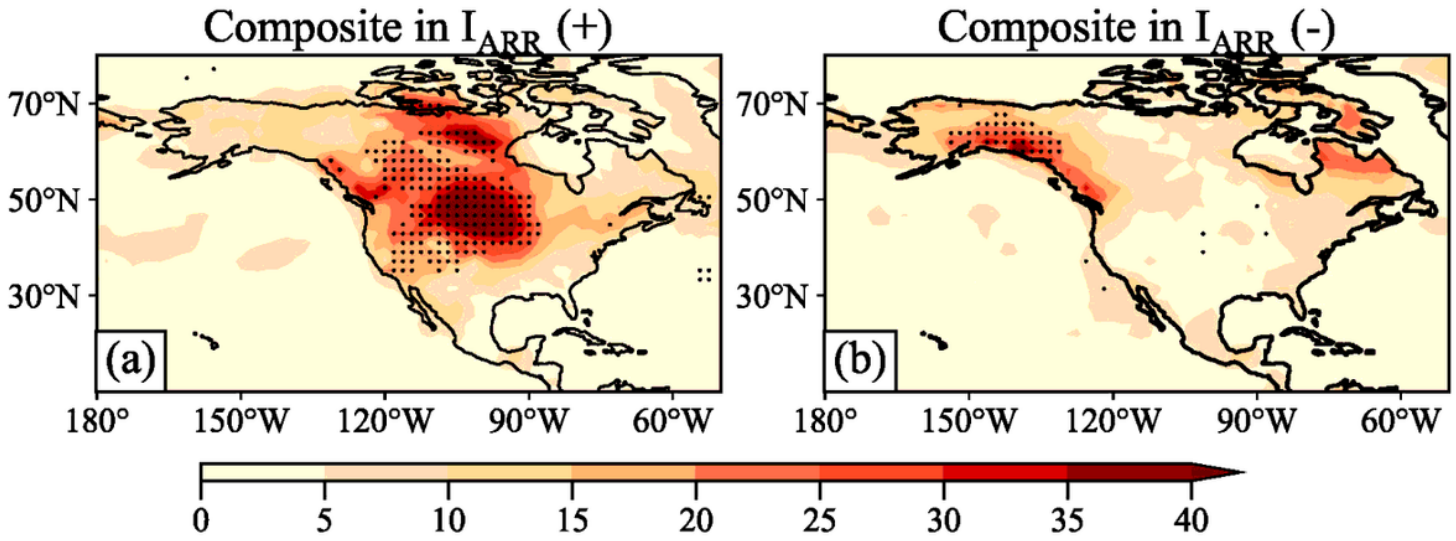

Figure 4

The composite patterns of the monthly integrated intensity of the extreme heatwave events are shown in shading (units: °C; interval: 5°C) contrasted (a) I_{ARR}>1 with (b) I_{ARR}< -1. The significances at 95% confidence level are marked by black dots. See more details about composite analysis and PDFs in Section 2.3.

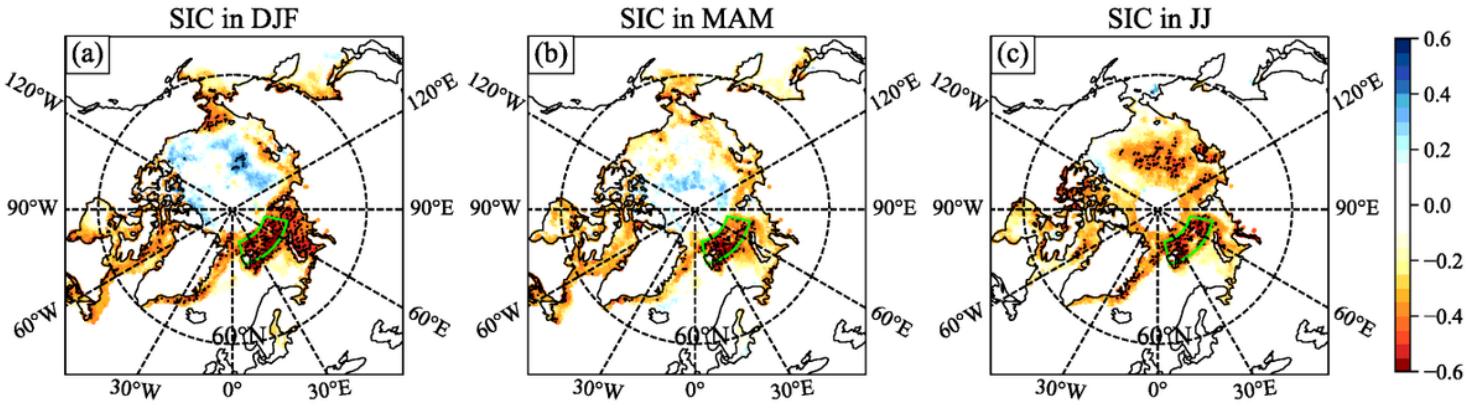

Figure 5

The correlation coefficients between I_{ARR} and SIC in (a) previous winter, (b) spring, and (c) early summer are shown in shading (interval: 0.05). The location (78°N -83 °N, 12°E -78 °E) marked with a green box in each pattern is the area used to calculate the I_{SIL} in each season at Fig. 6. The black dots denote the areas that are significant at above 99% confidence level. The blank center around the North Pole indicates the missing values of SIC.

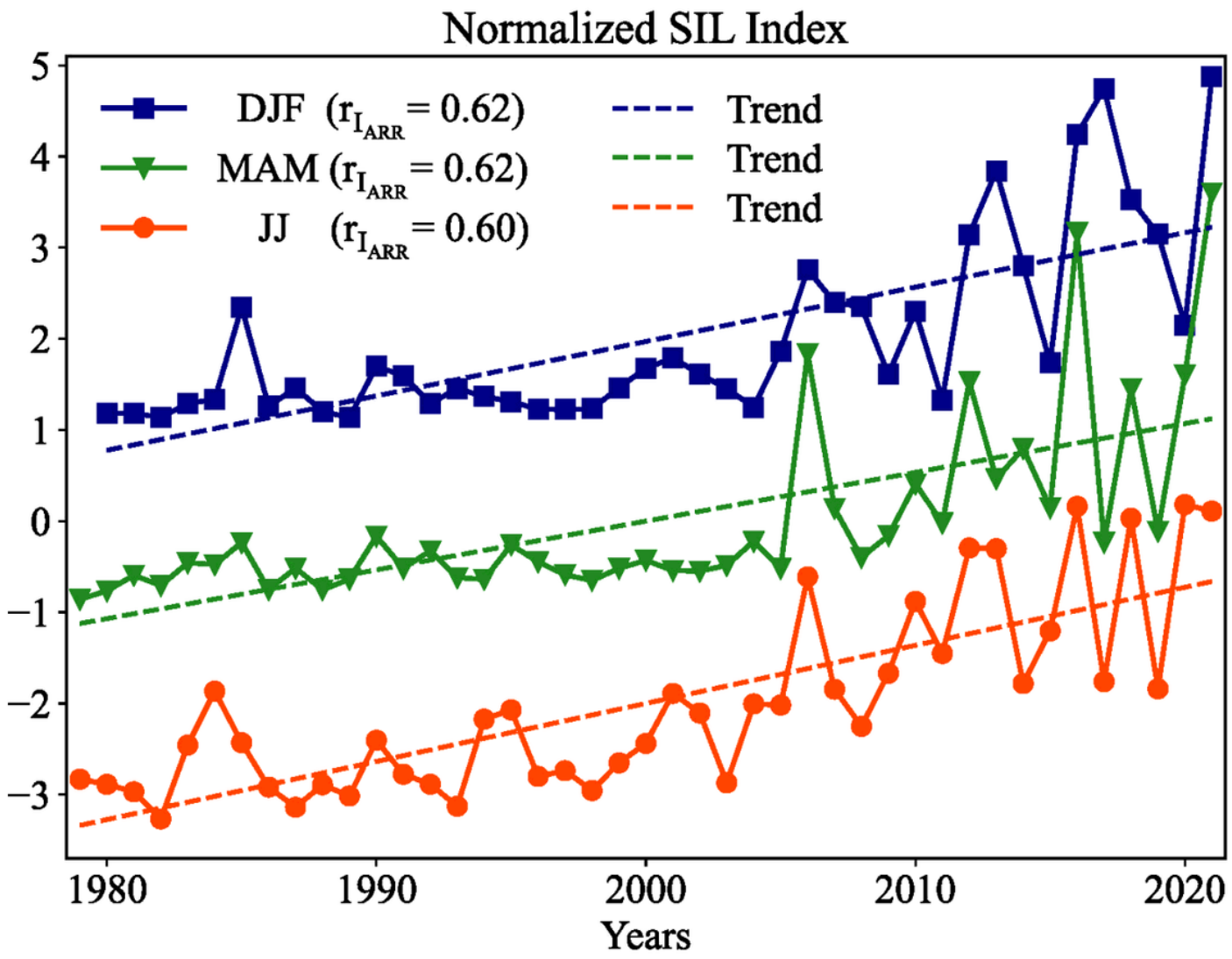

Figure 6

The normalized seasonal mean I_{SIL} in winter (navy line; offset by +2), spring (green line) and early summer (orange line; offset by -2) along with their linear trends (dotted line in their colors). The correlation coefficients between I_{ARR} and I_{SIL} in previous winter, spring, early summer are 0.62 ($p<0.01$), 0.62 ($p<0.01$), 0.60 ($p<0.01$), respectively.

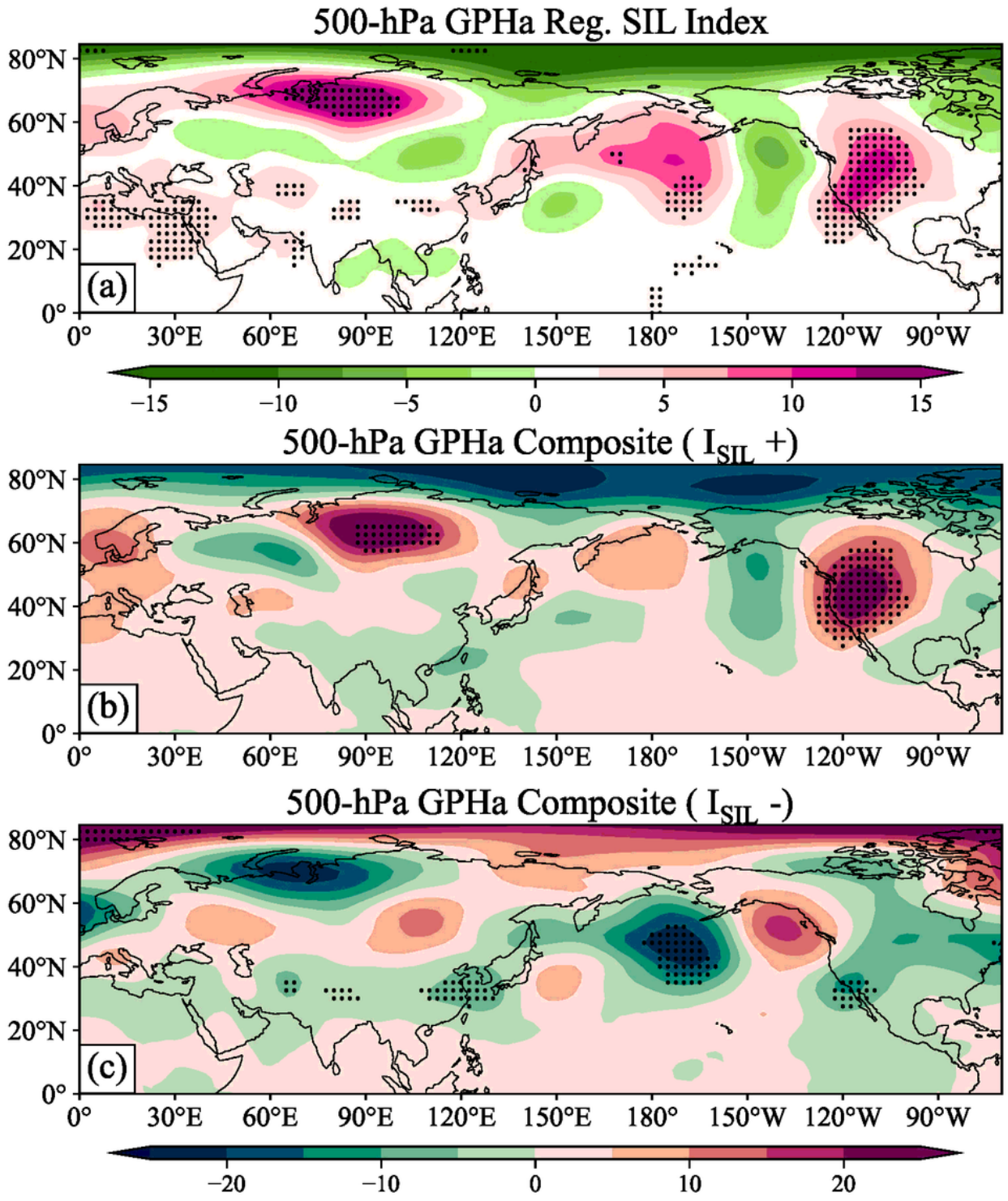

Figure 7

(a) The pattern of summertime 500-hPa GPHa regressing onto the I_{SIL} (units: gpm; interval: 2.5 gpm). The 500-hPa GPHa composite patterns (units: gpm; interval: 5 gpm) are shown in (b) and (c) contrasted I_{SIL} > 0.8 with I_{SIL} < -0.8, respectively. The black dots denote the areas that are significant at above 95% confidence level.

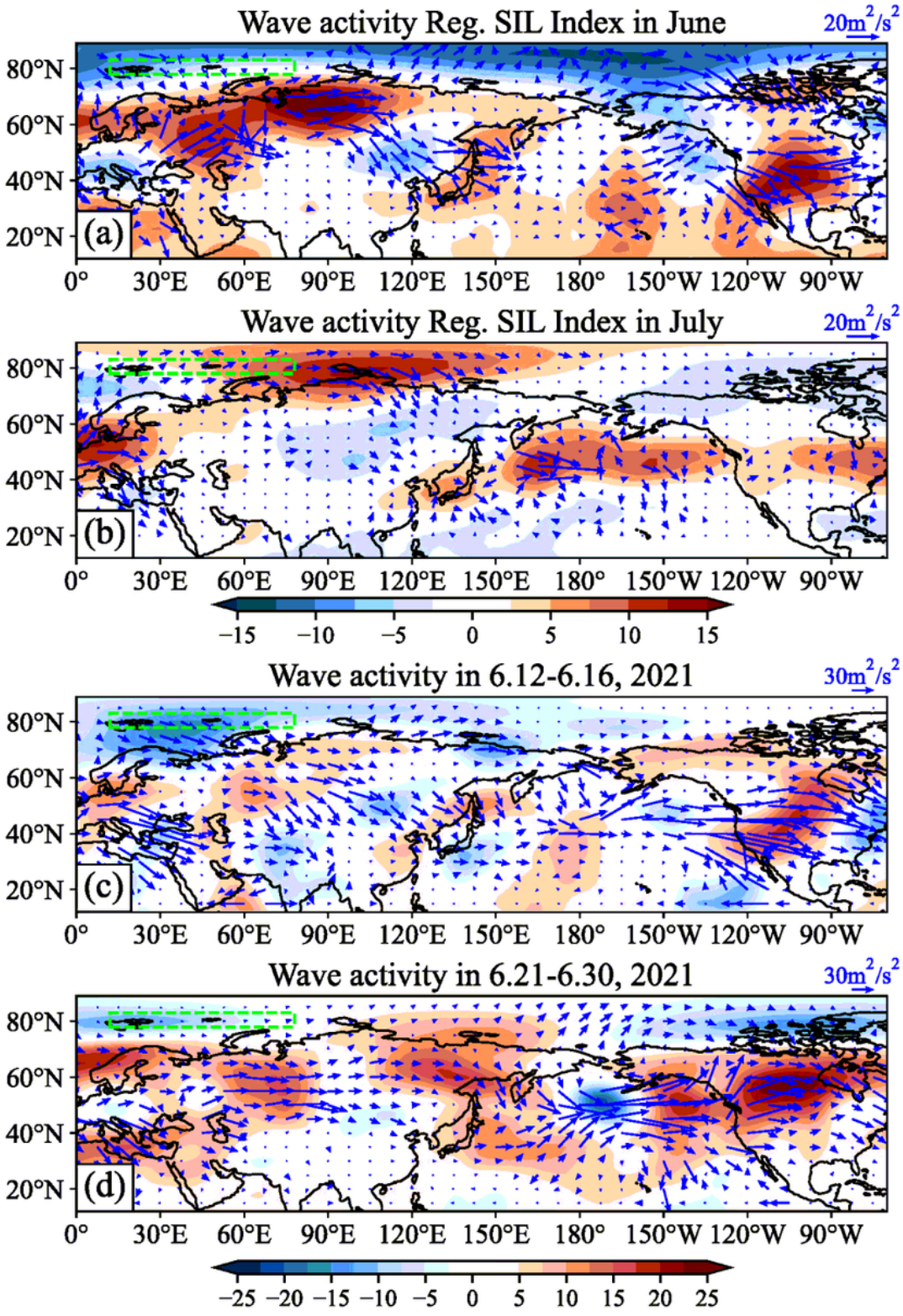

Figure 8

The atmospheric wave activity fluxes (vectors; units: m^2/s^2) and perturbation stream function (see Section 2.4 for details) at 500-hPa (shading; units: 10^6 m^2/s; interval: 2.5×10^6 m^2/s) associated with I_{SIL} in June (a) and July (b). The location marked with a lime box donates the same area in Fig. 5 to calculate

I_{SIL}. Panels (c,d) as in (a,b), but for atmospheric wave activity fluxes on 12-16 June, 2021 and 21-30 June, 2021.

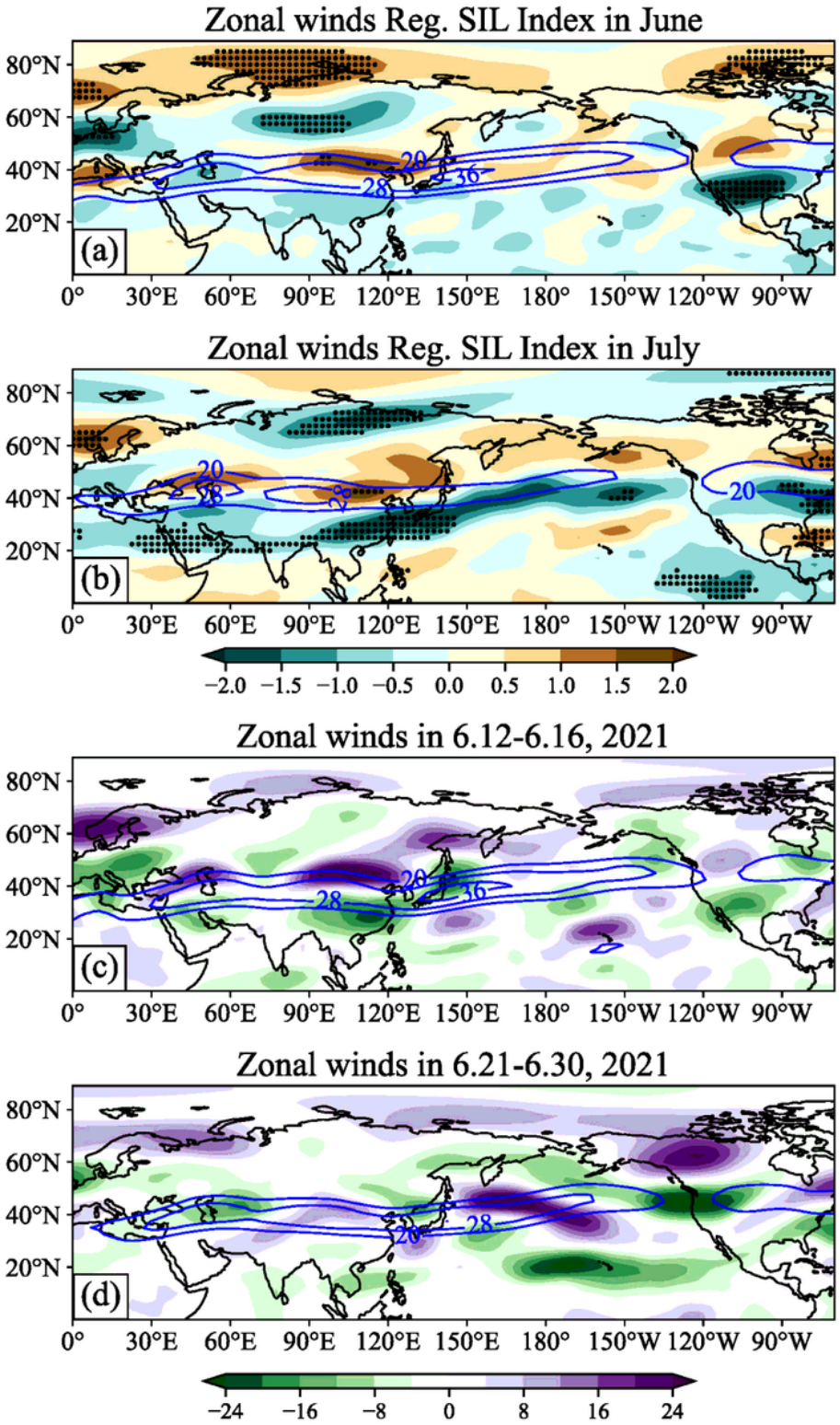

Figure 9

The regressions (shading; units: m/s; interval: 0.5 m/s) of 200-hPa zonal winds anomalies onto the I_{SIL} in June (a) and July (b). The blue contours and black dots donate the climatology (interval 8 m/s) and the

areas that are significant at above 95% confidence level, respectively. Panels (c,d) as in (a,b), but for the zonal winds anomalies (shading; interval: 2 m/s) and climatology (contours; interval: 8 m/s) in 12-16 June, 2021 and 21-30 June, 2021.

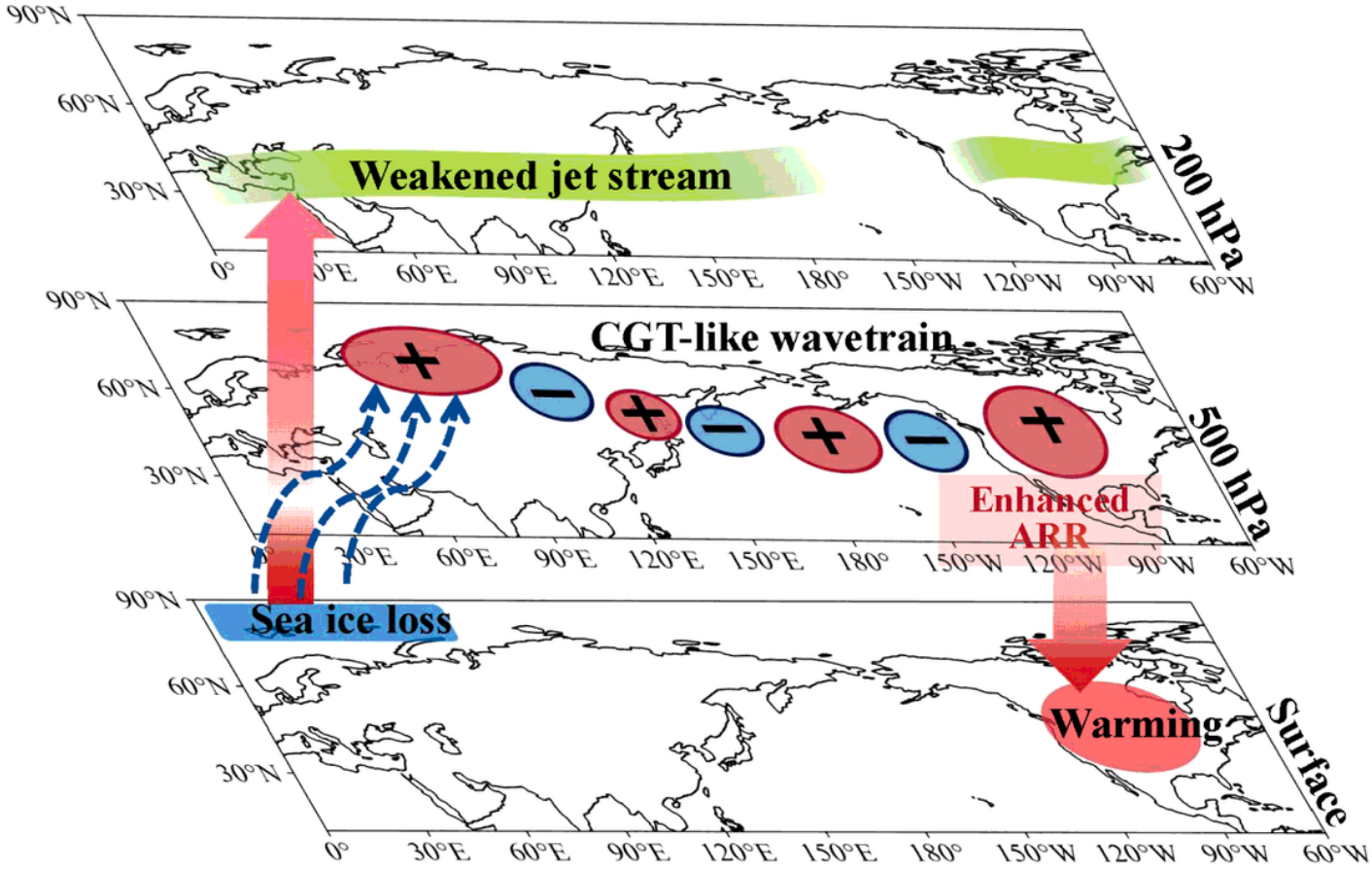

Figure 10

Schematic diagram for the mechanisms of Barents Sea ice loss influencing the atmospheric Rossby wave ridge and jet stream over western North America in the summertime, which eventually leads to heatwaves.